



# 3D In-Situ Characterizations of Damage Evolution in C/SiC Composite under Monotonic Tensile Loading by Using X-Ray Computed Tomography

Long Wang<sup>1</sup> · Wei Zhang<sup>1</sup> · Haibo Li<sup>1</sup> · Chuantao Hou<sup>1</sup> · Fang Ren<sup>1</sup>

Received: 31 October 2019 / Accepted: 26 February 2020 / Published online: 8 May 2020

© Springer Nature B.V. 2020

## Abstract

The damage evolution and fracture behavior in the bulk of C/SiC material under monotonic tensile loading have been investigated with the 3D in-situ observations by using X-ray CT. Crack initiated inside the matrix within 0.02 mm below surface when the load was only 19% of the failure strength, and propagated to the surface of matrix and towards the interior of specimen by breaking fibers and matrix when the load was above the elastic limit. With the further increasing of loading, other fiber breaks, matrix breaks and delaminations were observed to initiate and propagate both on the surface and in the bulk of specimen, while the cracks nucleating in the bulk of specimen are generally located at the laminae with a high volume fraction of pores. With the further propagations of cracks, the specimen split in the laminae with a large quantity of pores, while the fiber drawings results in the final fracture in the laminae without a large quantity of pores. The novel method being proposed to characterize the distribution of pores in this paper highlights the relation between the distribution of pores in the bulk of the studied material and cracks initiations and final fracture.

**Keywords** X-ray computed tomography · In-situ observations · C/SiC composite · Damage evolution · Fracture

## Highlights

- The damage evolution and fracture behavior in the bulk of C/SiC material under monotonic tensile loading have been investigated with the 3D in-situ observations by using X-ray CT.
- Crack initiated inside the matrix within 0.02 mm below surface when the load was only 19% of the failure strength, and propagated to the surface of matrix and towards the interior of specimen by breaking fibers and matrix when the load was above the elastic limit.
- A novel method being proposed to characterize the distribution of pores in this paper highlights the relation of the distribution of pores in the bulk of the studied material to crack initiation and final fracture.

✉ Long Wang  
long.wang.fr@hotmail.com

<sup>1</sup> Science and Technology on Reliability and Environmental Engineering Laboratory, Beijing Institute of Structure and Environment Engineering, No.1 South Dahongmen Road, Fengtai District, Beijing 100076, China

## 1 Introduction

Carbon fiber-reinforced SiC-matrix composite (C/SiC composite), which is an important Fiber Reinforced Ceramic Matrix Composites (FRCMC), is being widely used in the field of aerospace thanks to its low density, excellent high-temperature sustainability, high specific stiffness and specific strength [1–6]. A good understanding of the damage micromechanisms in C/SiC composite is crucial for the improvement of fabrication process and life predictions, and thus helps to ensure the security, the integrality and the reliability of composite structures [7, 8]. However, C/SiC composite has the complex three-dimensional microstructures in the bulk [8, 9], and pores that generally cannot be avoided in C/SiC composite material during some commonly used fabrication process, e.g. Chemical-Vapor Infiltration (CVI) process [2, 5, 10], form a three-dimensional interconnected network architecture [9, 10]. Thus the damage evolution in C/SiC composite are more complex. Therefore, it is necessary to characterize the damage evolution in the bulk of C/SiC composite directly by using the three-dimensional in-situ observation method [7, 8].

X-ray Computed Tomography (CT), which is a three-dimensional imaging facility, is able to characterize the microstructures in the bulk of material non-destructively [11, 12]. The three-dimensional image is reconstructed by using a set of radiographs that are recorded during the rotation of the sample mounted between the X-ray beam source and the detector. The gray levels in the reconstructed 3D image reflect the microstructural constituents in the bulk of sample. X-ray CT is being used as an attractive tool to follow the damage evolution in the bulk of sample in the field of experimental mechanics [12–18]. The special designed in-situ loading rigs allow the 3D images being recorded by X-ray CT during the mechanical tests. Thus the damage process in the bulk of sample could be revealed in the reconstructed 3D images. In this paper, this novel experimental method with three-dimensional in-situ observations has been used to characterize the complex damage and failure behaviors in C/SiC composite fabricated by CVI process under monotonic tensile loading in order to establish the relations of cracks initiations and propagations, delaminations and fracture behaviors with the microstructures and the pores in the bulk of specimen.

## 2 Experimental Methods

### 2.1 Material and Specimen

Two-dimensional plain woven C/SiC composite fabricated by CVI process has been studied. The T300 carbon fiber bundles are woven orthogonally ( $0^\circ/90^\circ$ ) in the plain. The previous three-dimensional characterization by using X-ray CT [9] has revealed the microstructures in the bulk of the material: the carbon fiber bundles, SiC matrix and pores could be segmented and rendered in 3D; the pores form a highly interconnected plain networks inside SiC matrix between laminae and even connect through several laminae to form a 3D interconnected network architecture. The specimen used in this paper was extracted from a C/SiC composite plate with the thickness of 3 mm (including about 17 layers). A small scan volume is necessary to ensure an high enough imaging resolution, thus the specimen with a small size of ROI (Region Of Interest) for the in-situ observations is used; the size of the specimen is shown in Fig. 1a.

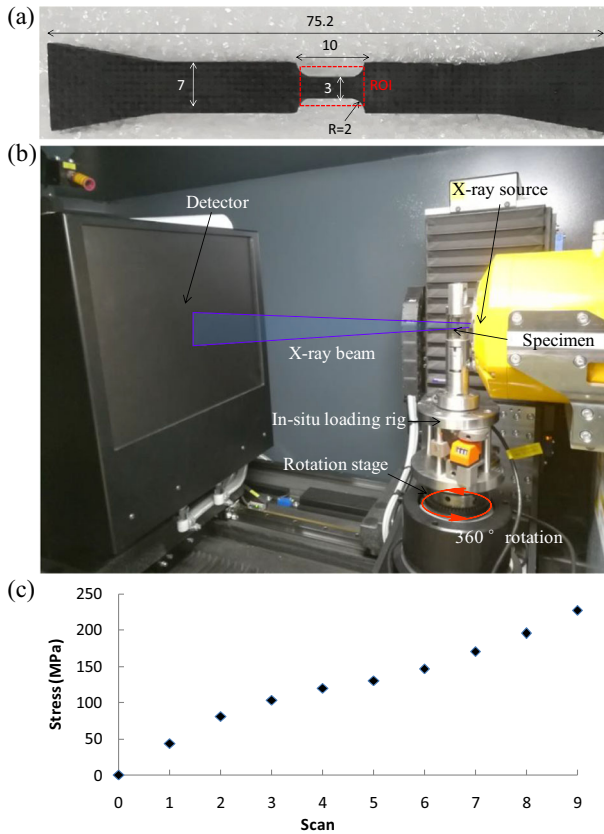


**Fig. 1** **a** The size of the specimen used for the in-situ tensile test (in mm), the ROI (Region Of Interest) is marked with a rectangle; **b** the experimental set-up for the monotonic tensile test with in-situ observations by using X-ray CT; **c** the scans performed during the pause of each step and after final failure

## 2.2 In-Situ Monotonic Tensile Test

A special designed in-situ loading device for X-ray CT was used to load the specimen. The maximum monotonic tensile loading provided by this device is about 3 KN. The device is supported by a tube made of quartz glass without obstructing the transmission of X-rays. The loading could be recorded by the sensor installed in the device while the displacement cannot be measured accurately by this device as well as some other homemade in-situ rigs [15, 17]. The specimen was installed in the device which is mounted on the rotating stage between the X-ray source and the detector (Fig. 1b). A series of projections (a scan) were recorded when the rotating stage is rotated around 360°, then a three-dimensional image were reconstructed using the recorded projections. The first scan was performed before loading in order to record the three-dimensional image of the undamaged specimen. The pores in the bulk of ROI were characterized qualitatively and quantitatively in 3D in order to ensure that the pores in the small size ROI could be representative of the studied material. Then the monotonic tensile loading was loaded step by step until final failure. The scans were performed at a constant load level during the pause of each step and after final failure in order to record the three-dimensional images under different loading status (Fig. 1c).

### 2.3 CT Observations and Data Analysis

The in-situ test was performed using a laboratory CT (Phoenix x|Nanotom m) fitted with a nanofocus X-ray tube. A 110 kV acceleration voltage was selected to ensure at least 10% transmission of the X-ray beam through the cross-section of the specimen. A set of 1600 radiographs (a scan) were taken while the specimen was rotated through  $360^\circ$  along its vertical axis. Two projections were taken at a given angular position: the first image was ignored to avoid the afterglow effect of the detector. With an acquisition time per projection of 1000 ms one scan lasted about 53 min. The resolution used in this paper is  $5.25 \mu\text{m}/\text{voxel}$ . Reconstruction of the tomographic data was performed with a filtered back-projection algorithm in order to obtain the 16 bit 3D digital images. The size of the saved 3D images is  $700 \times 1400 \times 2300$  voxel, and it is able to cover the whole ROI volume (Fig. 1a) between the two notches.

A necessary image registration with rigid translation was performed preliminarily to each 3D image obtained under different loading status. The analysis of CT image was performed slice by slice from different views. Image filtering, segmentation, 3D rendering and quantitative analysis were also used for the data analysis; the reader could refer to [9] for more details.

## 3 Results

The pores in the small size ROI of specimen were segmented and analyzed qualitatively and quantitatively (Fig. 2). The volume fraction of pores is about 10%. The pores are generally highly interconnected to form a 3D network architecture. The majority of pores are connected: they are marked with blue color in Fig. 2 and they occupy 89% volume of the total pores in the ROI. Thus the volume fraction and the morphology of pores in the small size ROI could be considered to be representative compared with the pores in a large volume in [9].

The specimen fractured at 227.4 MPa ( $\sigma_f$ ) under the monotonic tensile loading, and it is consistent with the ultimate strength (220~240 MPa) of the studied material. Figure 3 shows the 3D rendering of the specimen after failure, the final fracture is located in the middle of ROI between notches. As shown in Fig. 3, the plain (xz plain) that parallels to the laminae (xz plain)

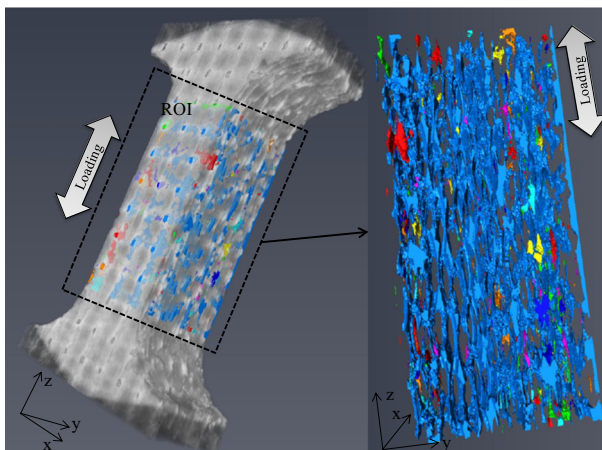


**Fig. 2** 3D rendering of the undamaged specimen (translucence) and the pores (colored) in the ROI

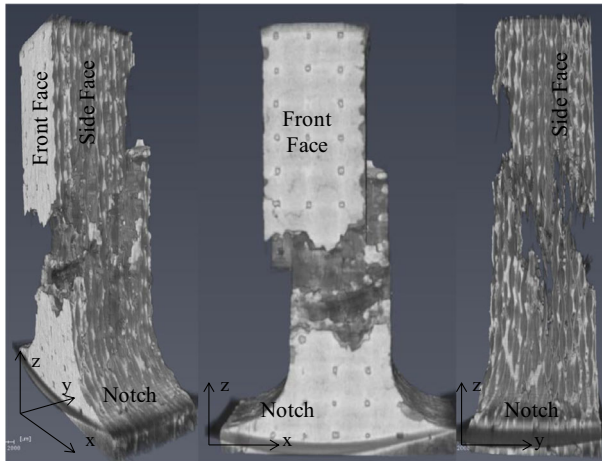


**Fig. 3** 3D rendering of the specimen after final failure

is defined as “Front” face in this paper; the plain ( $yz$  plain) that is perpendicular to the laminae and parallels to the loading direction (direction  $z$ ) is defined as “Side” face. The in-situ scans performed to the specimen and their relations with loadings are shown in Fig. 1c and listed precisely in Table 1. The damage evolution are analyzed step by step from different views in the following.

As shown in Fig. 4, the first crack initiation was observed at the load of 43.5 MPa ( $19\%\sigma_f$ ). The crack initiated at the interface (about 0.02 mm below the front surface) between surface SiC matrix and carbon fiber bundles (Fig. 4b). It is only a subsurface matrix break while no fiber break or surface matrix break was observed. This crack is called as “Main crack” in this paper. With the increasing of loading, the main crack was observed to propagate in the plain ( $xz$  plain) parallel to the laminae inside the surface matrix (Fig. 4c) at the load of 81.4 MPa ( $36\%\sigma_f$ ). It is still a subsurface matrix break (about 0.02 mm below the front surface) while no fiber break or surface matrix break (Fig. 4d) was observed. Once the load was increased to 103.1 MPa ( $45\%\sigma_f$ ), the main crack was observed to begin to propagate along the direction (direction  $y$ ) perpendicular to the laminae. It propagated to the specimen surface and the matrix break was observed on the surface in Fig. 4e. It also propagated towards the interior of the specimen simultaneously (Fig. 5) to break a  $0^\circ$  fiber bundle<sup>1</sup> at first and then induce a series of fiber breaks and matrix breaks.

Figure 5 shows the damage evolution in the representative CT slices parallel to the side face ( $yz$  plain, 0.14 mm below the surface). With the increase of loading (119.5 MPa ( $45\%\sigma_f$ ) ~ 195.5 MPa ( $86\%\sigma_f$ )), the main crack continued to propagated towards the interior of the specimen by breaking fiber bundles and matrix. In the same time, other fiber cracks and matrix cracks began to initiate and propagate in the bulk of the specimen: some of them resulted in the final failure, while the others did not. Crack 1 was observed to initiate by breaking surface matrix and a  $90^\circ$  fiber bundle at the load of 170.7 MPa ( $75\%\sigma_f$ ), and was then observed to propagate towards the interior of the specimen at the load of 195.5 MPa ( $86\%\sigma_f$ ). When the load arrived at 227.4 MPa ( $100\%\sigma_f$ ), Crack 1 resulted in the final fracture. However, Crack 2,

<sup>1</sup> The fiber bundle parallel to the loading direction is called as “ $0^\circ$  fiber bundle”, while the fiber bundle perpendicular to the loading direction is called as “ $90^\circ$  fiber bundle”.

**Table 1** The in-situ scans performed to the specimen and their relations with loadings

| In-situ loading/Scan  |   | 1    | 2    | 3     | 4     | 5     | 6     | 7     | 8     | 9     |
|-----------------------|---|------|------|-------|-------|-------|-------|-------|-------|-------|
| Mechanical Parameters | Stress (MPa)                                    | 43.5 | 81.4 | 103.1 | 119.5 | 130.3 | 146.6 | 170.7 | 195.5 | 227.4 |
|                       | Ratio to the fracture strength ( $\sigma_f\%$ ) | 19%  | 36%  | 45%   | 53%   | 57%   | 64%   | 75%   | 86%   | 100%  |

that had already been observed to initiate at the load of 146.6 MPa (64% $\sigma_f$ ) by breaking surface matrix and a 90° fiber bundle and propagate towards the interior of the specimen with the increase of loading, did not result in the final fracture. Similarly, Crack 3 was observed to initiate at the matrix between two laminae at the load of 119.5 MPa (53% $\sigma_f$ ) and propagate between two laminae. The delamination was observed due to the propagation of Crack 3 when the load arrived at 170.7 MPa (75% $\sigma_f$ ), and was observed to grow when the load increased to 195.5 MPa (86% $\sigma_f$ ). However, Crack 3 did not result in the final fracture when the specimen fractured at the load of 227.4 MPa (100% $\sigma_f$ ). Figure 6 shows another group of CT slices below surface to compare the damages at the load of 195.5 MPa (86% $\sigma_f$ ) and final fracture: although several cracks had been observed at the load of 195.5 MPa (86% $\sigma_f$ ), some of them did not result in the final fracture.

When the load was increased from 195.5 MPa (86% $\sigma_f$ ) to 227.4 MPa (100% $\sigma_f$ ), the main crack and Crack 1 propagated to two laminae with a large quantity of pores and resulted in the final failure of specimen. Figure 7 shows the relations between the quantitative analysis of pores and the final fracture behavior. A novel method has been proposed to characterize the distribution of pores in the studied material. The pores segmented in the ROI (Fig. 2) are quantified to show the distribution of volume fraction along the direction x (the top field shown in Fig. 7c) and the distribution of volume fraction in the different laminae (the bottom curve shown in Fig. 7c). When the main crack propagated (from right surface to the interior of specimen in Fig. 7) to the lamina “L14” with a high volume fraction of pores, the specimen split along the lamina “L14”. When Crack 1 propagated (from left surface to the interior of specimen in Fig. 7) to the lamina “L2” that has a higher volume fraction of pores than its

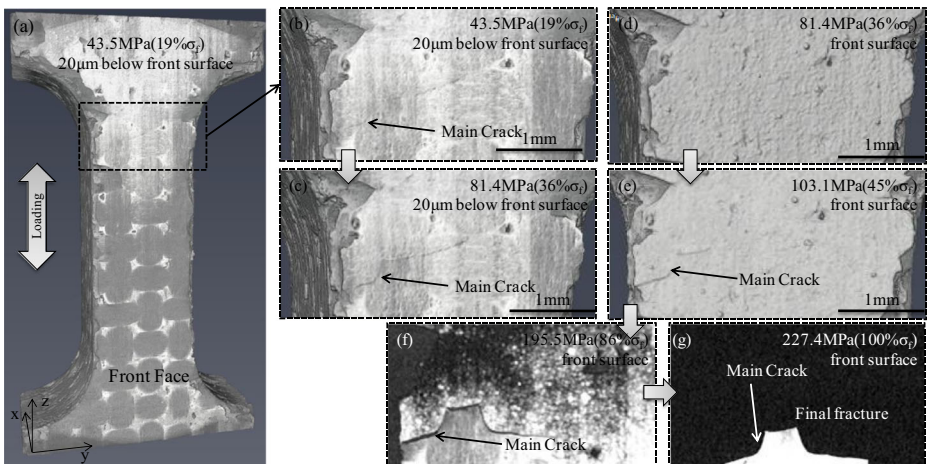


**Fig. 4** CT slices show the initiation and propagation of the main crack on the front surface and 0.02 mm below the front surface

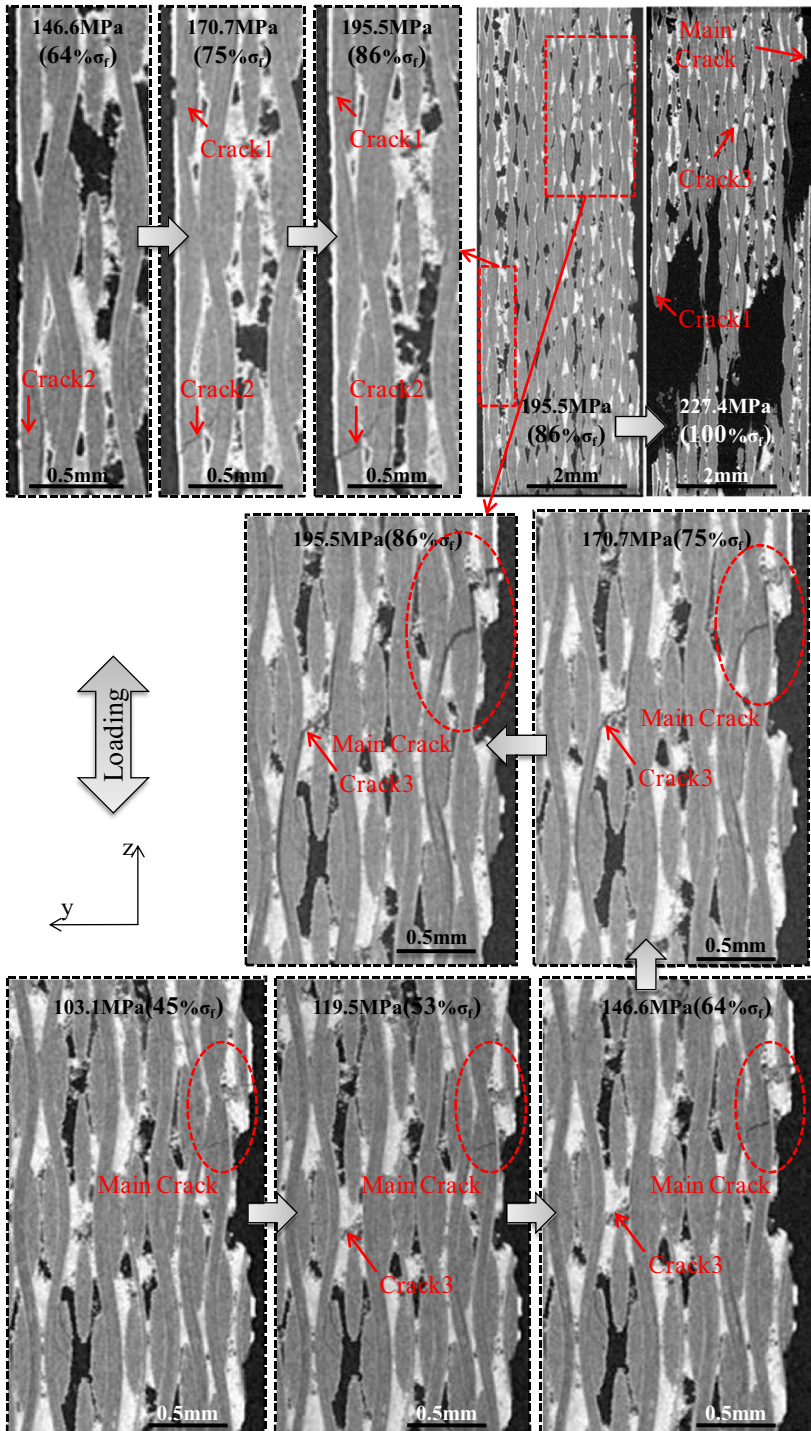
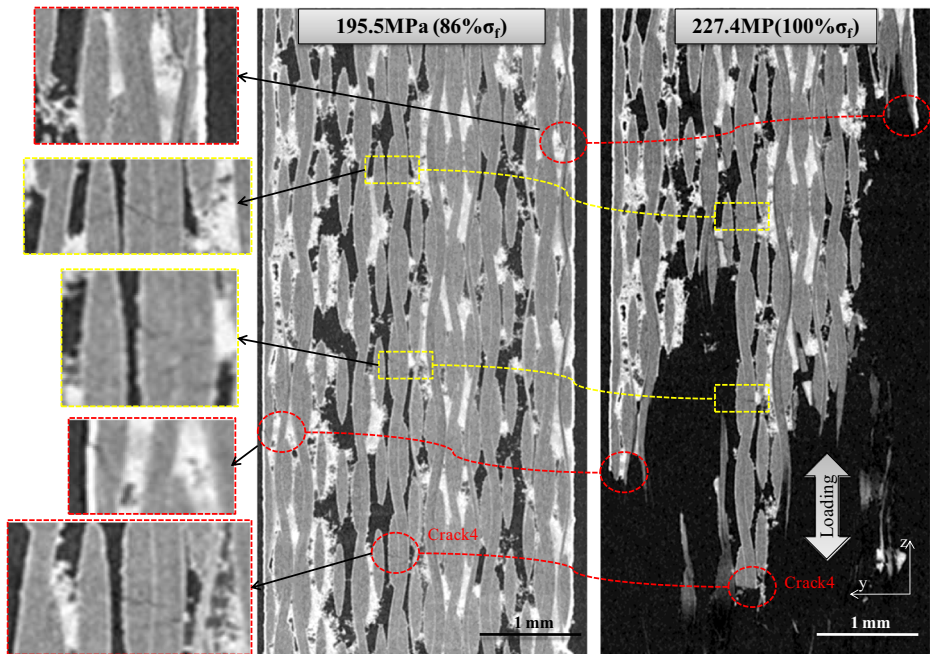


Fig.5 A group of CT slices show the damage evolution in the bulk of specimen (the CT slices are parallel to the side face (yz plain, 0.14 mm below the surface))



**Fig. 6** The comparisons between the damages at the load of 195.5 MPa ( $86\%\sigma_f$ ) and the final fracture for another representative CT slice parallel to the side face ( $yz$  plain, 2.1 mm below the CT slice shown in Fig. 5, 0.74 mm below the side face). The damages that resulted in the final fracture are marked with red circles, while the damages that did not result in the final fracture are marked with yellow rectangles

neighbor laminae “L1” and “L3”, the specimen fractured. The 3D rendering of the fractured specimen shown in Fig. 7a shows the fiber drawings close to the lamina “L2”, and it indicates that the final fracture did occur at the lamina “L2” due to the propagation of Crack 1. While between laminae “L2” and “L14”, the final fracture was found to be along the two laminae with high volume fraction of pores, i.e. “L4” and “L7”. Crack 4, that was observed at the load of 195.5 MPa ( $86\%\sigma_f$ ) in Fig. 6, is just located in the lamina “L7” where the specimen split in the middle.

## 4 Discussions

The damage evolution and fracture behavior in the studied C/SiC composite under monotonic tensile loading are summarized in Fig. 8. Crack was observed to initiate at matrix below surface when the load was only at 43.5 MPa ( $19\%\sigma_f$ ) and did not propagate to the surface until the load arrived at 103.1 MPa ( $45\%\sigma_f$ ). It is impossible to reveal this damage process by using the traditional experimental method with two-dimensional in-situ observations on surface. When the load was increased to 103.1 MPa ( $45\%\sigma_f$ ), fiber breaks were observed. The standard mechanical test performed on the studied material shows that the inelastic deformation begins when the load is above 90–100 MPa (elastic limit). It implies the relations between the inelastic deformation in the macro-scale and the fiber breaks in the micro-scale.

When the load was above the elastic limit, in addition to the propagation of the main crack, the other cracks began to initiate in the bulk of specimen with the increase of loading.



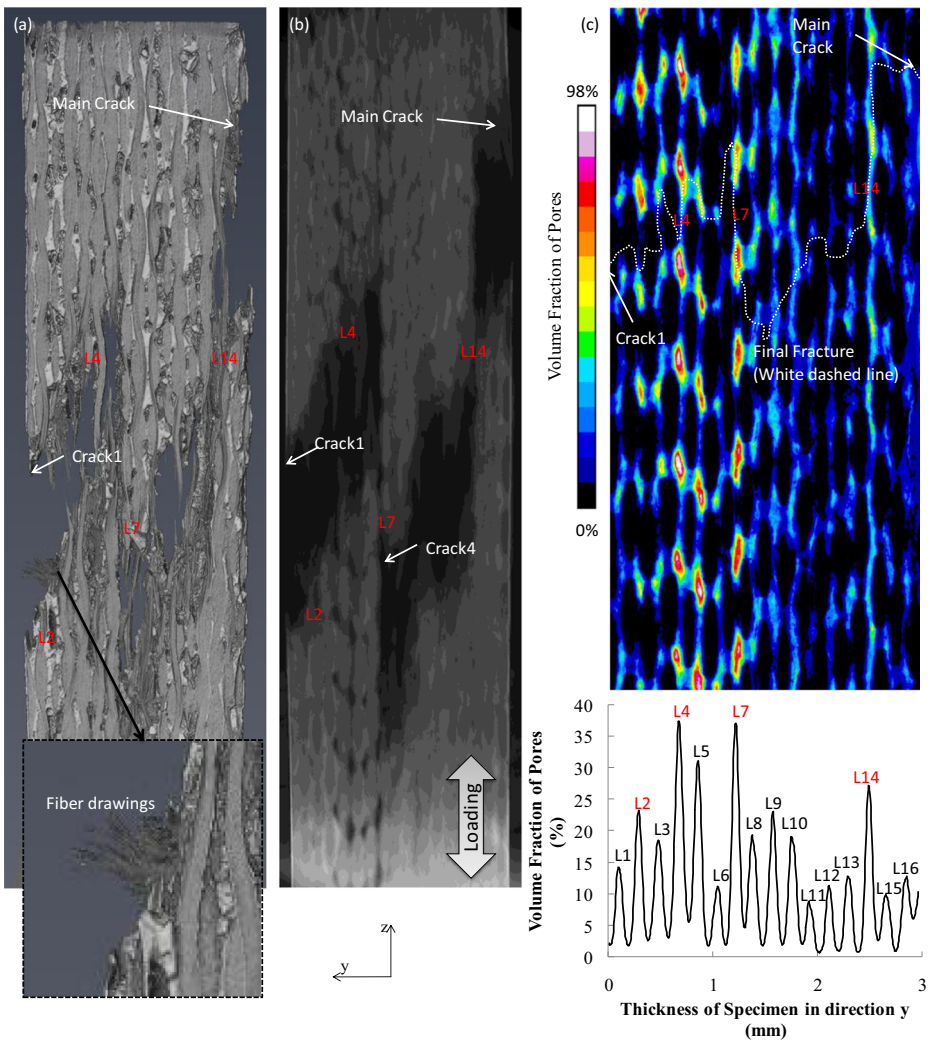


**Fig. 7** The comparisons between the fracture behavior and the distribution of pores in the bulk: **a** 3D rendering of the fractured specimen; **b** the projection of the final fractured specimen shown in (a); **c** the field in the top shows the distribution of the volume fraction of pores along the direction perpendicular to the yz plain, while the curve in the bottom shows the relations between the volume fraction of pores and the thickness of specimen (along the direction y). “Li” is used to number the laminae

These cracks can be classified as two categories: a) cracks nucleating on surface, e.g. Crack 1 and 2 in Fig. 5 and surface crack in Fig. 6; b) cracks nucleating in the interior of specimen, e.g. Crack 3 in Fig. 5 and Crack 4 and the other two cracks marked with yellow rectangles in Fig. 6. Specimen surface is prone to induce stress concentrations, thus the cracks nucleating on surface may be ascribed to the stress concentrations on surface. While the cracks nucleating in the interior of specimen in Fig. 6 (Crack 4 and the other two cracks marked with yellow rectangles) are located at the lamina “L7” that has a quite high volume fraction of pores in Fig. 7c. Stress concentrations are apt to be generated around pores. Thus it implies the relations between the initiations of these cracks and the distribution of pores. The results in [19, 20]

| Ratio to fracture strength<br>( $\sigma_f$ %) | Damage and fracture behaviors   |
|---|---|
| 19%   | <ul style="list-style-type: none"> <li>Main Crack initiated at matrix (the interface between surface SiC matrix and carbon fiber bundles, about 0.02 mm below the front surface, <b>INVISIBLE on surface</b>)</li> </ul>  |
| 36%   | <ul style="list-style-type: none"> <li>Main Crack propagated in the plain parallel to the laminates inside the surface matrix (<b>INVISIBLE on surface</b>)</li> </ul>  |
| 45%<br><i>Inelastic deformation</i>           | <ul style="list-style-type: none"> <li>Main Crack propagated to the surface (<b>VISIBLE on surface</b>)</li> <li>Main Crack propagated towards the interior to break fibers (<b>FIBER BREAKS occur</b>)</li> </ul>  |
| 53%-86%                                       | <ul style="list-style-type: none"> <li>Main Crack continued to propagate towards the interior to break fibers and matrix</li> <li>In additional to the Main Crack, other damages (Fiber breaks, Matrix breaks, Delaminations) initiated and propagated: some of them resulted in the final fracture, the others did not.</li> </ul>   |
| 100%  | <ul style="list-style-type: none"> <li>Cracks propagated to the laminates with <b>high volume fraction of pores</b> and resulted in the final fracture.</li> <li>Specimen fractured at some propagated cracks and split in the laminates with a <b>large quantity of pores</b>, while the <b>fiber drawings</b> resulted in the final fracture in the laminates without a large quantity of pores.</li> </ul> |

**Fig. 8** Summary of the damage and fracture behaviors in the studied C/SiC composite under monotonic tensile loading

show that the distribution of pores indeed has an influence on the macro mechanical property of carbon reinforced composite material. The experimental field measurement and numerical simulation [12, 15] are expected to validate the relations between the stress concentrations induced by the distribution of pores and the initiations of cracks: the mechanical full field could be measured by using the Digital Volume Correlation (DVC) method [21, 22]; a high fidelity Finite Element (FE) model based on the real three-dimensional morphologies of pores from CT image [8, 15, 23] could be used for the numerical simulation.

The relations between the distribution of pores and the final fracture are also emphasized in this paper. With the propagations of the main crack initiating on surface and the cracks at the laminae with high volume fraction of pores, the specimen split along the laminae (L4, L7, L14) with large quantity of pores. Then the specimen fractured after the drawings of fibers when Crack 1 propagated to the lamina “L2”. However, the specimen did not split along the lamina “L2”. This may be due to the lower volume fraction of pores in “L2” compared with “L4, L7 and L14” (Fig. 7).

## 5 Conclusions

The damage evolution and fracture behavior in the bulk of C/SiC material under monotonic tensile loading have been investigated in this paper with the three-dimensional in-situ observations by using X-ray CT:

- (1) Crack initiated inside the matrix within 0.02 mm below surface when the load was only 19% of the failure strength, and propagated inside the surface matrix along the plain parallel to the laminae; when the load was above the elastic limit, it propagated to the surface of matrix and towards the interior of specimen by breaking fibers and matrix.
- (2) With the further increasing of loading, other fiber breaks, matrix breaks and delaminations were observed to initiate and propagate both on the surface and in the bulk of specimen, while the cracks nucleating in the bulk of specimen are generally located at the laminae with a high volume fraction of pores.
- (3) With the further propagations of cracks, the specimen split in the laminae with a large quantity of pores, while the fiber drawings resulted in the final fracture in the laminae without a large quantity of pores.

The novel method being proposed to characterize the distribution of pores in this paper highlights the relation between the distribution of pores in the bulk of the studied material and cracks initiations and final fracture. It is expected to be validated in further based on the experimental full-field measurements using DVC method and the numerical simulations using a high fidelity FE model from CT image.

**Acknowledgments** The authors would like to thank Dr. Daxu Zhang (Shanghai Jiaotong University, Shanghai, China) for providing the in-situ loading rig.

## References

1. Mei, H., Han, D., Farhan, S., Cheng, L., Xu, H., Liu, Y.: Impact behavior of different cross-ply laminated carbon fiber-reinforced silicon carbide composites under the low velocity. *J. Compos. Mater.* **50**, 1137–1142 (2015)
2. Xu, Y., Ren, S., Zhang, W.: Thermal conductivities of plain woven C/SiC composite: Micromechanical model considering PyC interphase thermal conductance and manufacture-induced voids. *Compos. Struct.* **193**, 212–223 (2018)
3. Yang, W., Zhang, L., Cheng, L., Liu, Y., Cheng, L., Zhang, W.: Oxidation behavior of C/SiC composite with CVD SiC-B<sub>4</sub>C coating in a wet oxygen environment. *Appl. Compos. Mater.* **16**, 83–92 (2009)
4. Zhao, L., Yang, W., Cao, T., Li, H., Liu, B., Zhang, C., Zhang, J.: A progressive failure analysis of all-C/SiC composite multi-bolt joints. *Compos. Struct.* **189**, 378–385 (2018)
5. Naslain, R.: Design, preparation and properties of non-oxide CMCs for application in engines and nuclear reactors: an overview. *Compos. Sci. Technol.* **64**, 155–170 (2004)
6. Liu, Y., Cheng, L., Zhang, L., Yang, W., Zhou, S., Zhang, W.: Abrication and mechanical behaviors of 2D C/SiC-BCx composite at room temperature. *J. Compos. Mater.* **46**, 1251–1260 (2011)
7. Bale, H.A., Haboub, A., MacDowell, A.A., Nasiatka, J.R., Parkinson, D.Y., Cox, B.N., Marshall, D.B., Ritchie, R.O.: Real-time quantitative imaging of failure events in materials under load at temperatures above 1600°C. *Nat. Mater.* **12**(1), 40–46 (2013)
8. Marshall, David, Cox, Brian, Kroll, Peter, Hilmas, Greg, Fahrenholtz, William, Raj, Rishi, Ritchie, Robert, Yang, Qingda, Zok, Frank. National Hypersonic Science Center for Materials and Structures. AD report, (2014)
9. Wang, L., Yuan, K., Luan, X., Li, Z., Feng, G., Jianguo, W.: 3D characterizations of pores and damages in C/SiC composites by using X-ray computed tomography. *Appl. Compos. Mater.* **26**, 493–505 (2019)
10. Feng, Y., Feng, Z., Li, S., Zhang, W., Luan, X., Liu, Y., Cheng, L., Zhang, L.: Micro-CT characterization on porosity structure of 3D Cf/SiCm composite. *Compos. Part A.* **42**, 1645–1650 (2011)
11. Salvo, L., Suéry, M., Marmottant, A., Limodin, N., Bernard, D.: 3D imaging in material science: application of X-ray tomography. *Comptes Rendus Phys.* **11**, 641–649 (2010)
12. Wang, L., Guolin, F., Zhiqiang, L., Wu, J., Wei, Z.: Applications of X-ray computed tomography to study the mechanical behaviors of materials. *Struct. Environ. Eng.* **44**, 43–56 (2017)

13. Buffiere, J.-Y., Maire, E., Adrien, J., Masse, J.-P., Boller, E.: In-situ experiments with X ray tomography: an attractive tool for experimental mechanics. *Exp. Mech.* **50**, 289–305 (2010)
14. Maire, E., Zhou, S., Adrien, J., Dimichiel, M.: Damage quantification in aluminium alloys using in situ tensile tests in X-ray tomography. *Eng. Fract. Mech.* **78**, 2679–2690 (2011)
15. Wang, L., Limodin, N., El Bartali, A., Witz, J.-F., Seghir, R., Buffiere, J.-Y., Charkaluk, E.: Influence of pores on crack initiation in monotonic tensile and cyclic loadings in lost foam casting A319 alloy by using 3D in-situ analysis. *Mater. Sci. Eng. A.* **673**, 362–372 (2016)
16. Proudhon, H., Buffière, J.-Y., Fouvry, S.: Three-dimensional study of a fretting crack using synchrotron X-ray micro-tomography. *Eng. Fract. Mech.* **74**, 782–793 (2007)
17. Limodin, N., El Bartali, A., Wang, L., Lachambre, J., Buffière, J.-Y., Charkaluk, E.: Application of X-ray microtomography to study the influence of the casting microstructure upon the tensile behaviour of an Al-Si alloy. *Nucl. Instrum. Methods Phys. Res. Sec. B: Beam Interact. Mater. Atoms.* **324**, 57–62 (2014)
18. Wu, S.C., Xiao, T.Q., Withers, P.J.: The imaging of failure in structural materials by synchrotron radiation X-ray microtomography. *Eng. Fract. Mech.* **182**, 127–156 (2017)
19. Xie, N., Smith, R.A., Mukhopadhyay, S., et al.: A numerical study on the influence of composite wrinkle defect geometry on compressive strength. *Mater. Des.* **140**, 7–20 (2018)
20. Liu, T., Sun, B., Bohong, G.: Influence of specimen size and inner defects on high strain rates compressive behaviors of plain woven composites. *Polym. Test.* **64**, 55–64 (2017)
21. Buljac, A., Jailin, C., Mendoza, A., Neggers, J., Taillandier-Thomas, T., Bouterf, A., Smaniotto, B., Hild, F.: Digital volume correlation: review of progress and challenges. *Exp. Mech.* **58**(5), 661–708 (2018)
22. Pan, B., Wu, D., Wang, Z.: Internal displacement and strain measurement using digital volume correlation: a least-squares framework. *Meas. Sci. Technol.* **23**, 045002 (2012)
23. Bacaicoa, I., Wicke, M., Luetje, M., Zeismann, F., Brueckner-Foit, A., Geisert, A., Fehlbier, M.: Characterization of casting defects in a Fe-rich Al-Si-Cu alloy by microtomography and finite element analysis. *Eng. Fract. Mech.* **183**, 159–169 (2017)

**Publisher's Note** Springer Nature remains neutral with regard to jurisdictional claims in published maps and institutional affiliations.